Structural Stability, Elasticity, Thermodynamics and Electronic Structures of L12-Type Ni3X (X=Al, Ti, V, Nb) Phases Under External Pressure Condition

Y H Wu
Shanghai University of Engineering Science
J S Chen (cjshbb@sjtu.edu.cn)
Shanghai University of Engineering Science https://orcid.org/0000-0002-5891-496X
J Y Ji
Shanghai University of Engineering Science
Y Z Zhang
AECC Commercial Aircraft Engine manufacturing Co.,Ltd
Q Z Wang
Shanghai Sany Heavy Machinery Co.,Ltd
K Xiong
Yunnan University

Research Article

Keywords: Ni3X, elastic constants, thermodynamic, electronic structures, First-principles

Posted Date: September 27th, 2021

DOI: https://doi.org/10.21203/rs.3.rs-868726/v1

Version of Record: A version of this preprint was published at Journal of Molecular Modeling on January 1st, 2022. See the published version at https://doi.org/10.1007/s00894-021-05014-6.

Structural stability, elasticity, thermodynamics and electronic structures of $L1_2$-type Ni_3X (X=Al, Ti, V, Nb) phases under external pressure condition

Y H Wu[a], J S Chen[a,b*], J Y Ji[a], YZ Zhang[c], Q Z Wang[d**], K Xiong[e]

[a] *School of Materials Engineering, Shanghai University of Engineering Science, Shanghai, People's Republic of China*

[b] *School of Materials Science and Engineering, Shanghai Jiao Tong University, Shanghai, People's Republic of China*

[c] *AECC Commercial Aircraft Engine manufacturing Co., Ltd, Shanghai 200241, People's Republic of China*

[d] *Shanghai Sany Heavy Machinery Co., Ltd, Shanghai 200241, People's Republic of China*

[e] *Materials Genome Institute, School of Materials and Energy, Yunnan University, Kunming 650091, P. R. China*

**E-mail: cjshbb@sjtu.edu.cn *Tel. and Fax: +86-21-67791474; **E-mail:wangqz4@sany.com.cn*

Abstract: In this paper, the impacts of external pressure on structural stability, elasticity, thermodynamics and relevant electronic structures of $L1_2$-type Ni_3X (X=Al, Ti, V, Nb) phases were investigated using the first-principles methods. The lattice parameters(a,b,c) and volume(V) of the Ni_3X phases decrease with increasing pressure. however, the elastic constants(C_{ij}), bulk modulus(B), shear modulus(G), and Young's modulus (E) increase. The calculated elastic constants indicate that the mechanical stability and ductility of Ni_3X phases enhance with increasing pressure. The mechanical anisotropy of Ni_3X phases are enhanced by the raised pressure. Electronic analysis shows that increase pressure makes Ni-d-orbital and X(X=Al, Ti, V, Nb) -d-orbital hybridization stronger and electron transfer increases. The sequence in regard to electron aggregation strength is Ni_3Ti>Ni_3Nb>Ni_3V>Ni_3Al. It is more directly reflected in the charge density difference maps. This is consistent with the analysis results of the enthalpy of formation(ΔH) and Debye temperature (Θ_D).

Keywords: Ni_3X; elastic constants; thermodynamic; electronic structures; First-principles

1. Introduction

Ni-based single-crystal superalloys are one the most important high- temperature materials. Which are widely used for modern aircraft engines owning to high

temperature strength[1], thermal stability [2-4], creep resistance [5,6] and oxidation resistance [7-9] at high temperatures. The excellent mechanical properties of nickel-based single-crystal superalloys at high temperatures are depend mainly on the effect of the γ′-Ni_3Al strengthening phase in the alloy [10]. The large number of investigations on the γ′-Ni_3Al strengthening phase were found that the strengthening effect cannot meet the requirements for the performance of nickel-based single crystal alloys under high temperature conditions any more [11-13]. Recent studies have proven the mechanical characteristics of nickel-based single crystal alloys can be significantly reinforced by adding Ti, V, Nb, Ta [11-13], and promotes the formation of the $L1_2$-type γ′-Ni_3X (X=Ti, V, Nb) phases.

Over the past decades, there are currently few reports on Ni_3Ti (Hexagonal), Ni_3V(Tetragonal), Ni_3Nb (Tetragonal), Ni_3Ta (Tetragonal). Li *et al.* [14] investigated the mechanical properties of γ″-Ni_3Ta under variable pressure by means of theoretical simulations, and explored the internal mechanisms affecting its stability and mechanical strength. K. Santhy *et al.*[15] identifies the phase of stability of Ni_3(Ti, V) through first principles calculations. Tomasz Czeppe *et al.* [16] research effects of Ti and high cooling rate on the phase equilibrium and properties of Ni_3(Al, V) alloys. Gong *et al.* [17] analyzed the effect of alloying elements on the occupation preference, structural stability and mechanical performance of γ″-Ni_3Nb based on density functional theory.

In recent research, the calculation of phases based on density functional theory mainly focused on under fixed conditions. For example, Hou *et al.* [18] calculated the structural, elastic, thermodynamic and electronic behaviour of Ni_3Al, Ni_3Ga and Ni_3Ge under assumed pressures. The elastic properties, thermodynamic stability, lattice anisotropy and Debye characteristic temperature of Ni_3X were found to increase with increasing external pressure. Mao *et al.* [19] explored the mechanical stability, microscopic electronic structure and thermodynamic properties of Mg_2Sr by applying different pressures. Liu *et al.* [20] investigated the impact of pressure on the microscopic crystal structure, electron distribution properties and bonding ion configuration of the $MgCu_2$ Laves phase. The results of Zhao *et al.* [21] showed that

the variation of pressure could improve the mechanical stability, microscopic electronic structure and thermodynamic properties of Ni_3V intermetallic compound and improve the mechanical strength of the alloy. Chen *et al.* [22] performed first-principles calculations on $D0_{22}$-type Al_3V and Al_3Nb intermetallic compounds and found that pressure has a profound effect on the structure, mechanical properties and electronic properties of Al_3V and Al_3Nb. These studies are reported to provide new ideas and directions for the study of material properties, and they provide new theoretical approaches for the design, development and stability of new materials.

Based on the above research reports, first-principles calculations was used to investigate the structural stability(ΔH), elastic constants(C_{ij}), bulk modulus (B), Yong's modulus (E), shear modulus (G), Debye temperature (Θ_D)，and electronic structures of L12-type Ni3X (X=Al, Ti, V, Nb) phases under external pressure condition. The aim of this work is to provide theoretical basis for the exploration of material structure, organization and properties of $L1_2$-type γ′-Ni_3X, and also provides important theoretical references for subsequent experimental studies and alloy design.

2. Model and Computational details

The $L1_2$-type γ′-Ni_3X (X = Al, Ti, V, Nb) phase has a face-centered cubic structure [23] (FCC) with space group P*m*-3*m* (No. 221). All calculations are conducted using the plane-wave-pseudopotential approach based on the DFT [24]. The generalized gradient approximation of the function PBE [25] is used to represent the electron exchange-related potential. The geometry of the primal unit of Ni_3X was optimized by the Broyden-Fletcher-Goldfarb-Shanno (BFGS) scheme [26]. The cutoff energy of the atomic wave function was set to 440 eV and the K-point was given as 8×8×8. The valence electron configurations of Ni-$3d^8 4s^2$, Ti-$3d^2 4s^2$, V-$3d^3 4s^2$, Nb-$4d^4 5s^1$, and Ta-$4f^{14} 5d^3 6s^2$ were regarded. The convergence tolerance was set to an energy of 2.0 × 10-5 eV/atom. The SCF convergence threshold was established at 2.0 × 10-6 eV/atom, with forces on an individual atom lower than 0.03 eV/Å, stress deviations smaller than 0.05 Pa, and tolerance biases shorter than 0.001 Å.

3. Results and discussion

3.1. Structural properties

The stability of a material is closely related to the enthalpy of formation of the crystals that make up the material. The enthalpy of formation is the total energy of the crystal minus the energy of the reactants. When the value of the enthalpy of formation is less than zero, it indicates that the crystal structure is thermodynamically stable; otherwise, the crystal structure is unstable. In this research, the enthalpy of formation (*ΔH*) of $L1_2$-type γ′-Ni_3X (X=Al, Ti, V, Nb) can be determined by the following expression.

$$\Delta_r H_m^\theta = \Delta_f H_m^\theta (product) + \Delta_f H_m^\theta (reac\tan t) \quad (1)$$

$$\Delta H = \frac{5eN_A}{2}\left[E_{Total}^{Ni_3X} - (3E_{Total}^{Ni} + E_{Total}^{X}) \right] \quad (2)$$

where $E_{Total}^{Ni_3X}$ represents the total energy of $L1_2$-type γ′-Ni_3X; N_A stands for Avogadro's constant; e is for the basic charge; E_{Total}^{Ni} and E_{Total}^{X} are the energy per atom in the Ni and X crystals, respectively.

The calculated values of the lattice parameters a, b, c, the formation enthalpy (*ΔH*), volume at 0 GPa, and experimental and theoretical data studied by other researchers are listed in Table 1. This indicates that the calculated lattice constants are less than 1% of the theoretical allowable error from the experimental[27] and theoretical data[15, 28-30]. The *ΔH* of $L1_2$-type γ′-Ni_3X (X=Al, Ti, V, Nb) phases at 0 GPa are -48.15, -53.05, -20.49, -21.82 kJ/mol, respectively. It indicates that $L1_2$-type γ′-Ni_3X phase is thermodynamically stable, the stability of the γ′-Ni_3X has following sequence: Ti> Al> Nb>V, and the *ΔH* of Ni_3Ti, Ni_3V are relatively close to -45.14 KJ/mol and -16.27 KJ/mol with previous research findings [15], indicating that the feasibility of the calculation method and the simulative results are accurate.

Table1 Lattice parameters and formation enthalpy (ΔH) of $L1_2$-type γ′-Ni_3X (X=Al, Ti, V, Nb) phase at 0 GPa.

Phase	Species	Lattice constant(Å)	V(Å^3)	ΔH(KJ/mol)
Ni_3Al	This study	a=b=c=3.577	45.753	-48.15
	Experiment [27]	a=b=c=3.572		
	Other calculation [28]	a=b=c=3.574		
Ni_3Ti	This study	a=b=c=3.621	47.494	-53.05

	Other calculation [29]	(Hexagonal)		-38.29
	Other calculation [15]	a=b=c=3.610		-45.14
Ni_3V	This study	a=b=c=3.746	52.570	-20.49
	Other calculation [30]	(Tetragonal)		-26.70
	Other calculation [15]	a=b=c=3.569		-16.27
Ni_3Nb	This study	a=b=c=3.696	50.498	-21.82
	Other calculation [31]	(Tetragonal)		-39.50

Fig. 1 shows the curves of lattice constants and cell volume (V) of $L1_2$-type γ′-Ni_3X as a function of pressure. It can be seen that a (a=b=c) and V decrease with the increase of pressure, indicating that the increase of pressure leads to the compression of cell volume and the atomic distances become smaller. However, as the pressure increases, the decrease in the interatomic distance slows down and the volume change becomes slow. This is due to the fact that the reduction of interatomic distances under high pressure disrupts the balance of interatomic interaction forces and leads to strong repulsion between atoms, which makes it difficult for the crystal to continue to be compressed under high pressure.

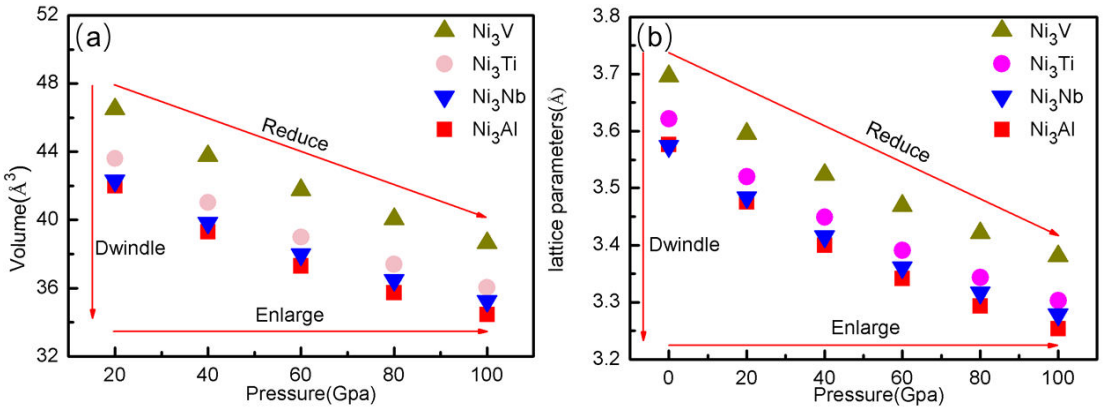

Fig.1 Variations of the lattice parameters and unit cell volume of $L1_2$-type γ′-Ni_3X (X=Ti, V, Nb, Ta) with 0 to 100GPa.

3.2. Elastic properties

The elastic constant is a physical quantity used to characterize the elastic properties of a material, and it has an extremely important influence on the overall performance of the material. This physical quantity makes it possible to correlate the mechanical properties of a material with its stiffness, mechanical stability and stress-strain relationship. Fig. 2 shows the trend of the elastic constants(C_{ij})of Ni_3X (X=Al, Ti, V, Nb) at 0 to 100GPa. It can be seen that the stability of Ni_3X phase under

external pressure satisfies the following constraints on the mechanical stability of cubic crystals [32-33]:

$$C_{11}-C_{12}>0, C_{11}>0, C_{44}>0, C_{11}+2C_{12}>0 \quad (3)$$

which indicates they are mechanically stable under compression. Furthermore, it is observed that C_{11}, C_{12} and C_{44} increase with pressure increasing, C_{11} possesses relatively large values, among which C_{11} is more sensitive to the change of pressure than C_{12} , C_{44}. Since C_{11} represents the elasticity in length, whereas C_{12} and C_{44} are on behave of the elasticity in shape, explain the off diagonal and elastic shear characteristic of cubic crystals [34], respectively. Under zero pressure, the C_{44} value of Ni_3Nb is the smallest and close to zero, it shows that Ni_3Nb have almost no shape elasticity at 0 GPa. The larger change in C_{11} is due to the strain on the length, which produces a certain volume change without changing the shape of the crystal.

Table 2 The elastic constants (C_{ij}), bulk modulus (B), Yong's modulus (E), shear modulus (G), Poisson's ratio (**v**) of Ni_3X (X=Al, Ti, V, Nb) at 0 to 100GPa.

Phase	P(GPa)	C_{11}	C_{12}	C_{44}	B	G	E	G/B	v
Ni_3Al									
	0	226.9	158.9	123.9	181.6	74.1	195.7	0.41	0.320
	20	306.0	239.3	165.0	261.6	88.2	237.9	0.34	0.348
	40	404.0	319.3	205.9	347.5	110.7	300.2	0.32	0.356
	60	506.5	409.0	243.0	441.5	129.5	353.9	0.29	0.367
	80	589.4	482.0	277.5	517.8	146.0	400.4	0.28	0.371
	100	650.1	534.7	310.3	573.1	161.0	441.6	0.28	0.372
Ni_3Ti									
	0	252.1	135.8	123.0	174.5	91.1	232.8	0.52	0.278
	20	374.8	228.2	160.3	227.1	117.1	299.8	0.51	0.280
	40	461.0	301.8	190.0	354.9	134.0	357.1	0.38	0.332
	60	558.8	374.4	218.7	435.8	154.7	415.0	0.35	0.341
	80	647.9	444.6	245.1	512.4	172.2	464.6	0.34	0.349
	100	731.7	515.0	272.2	587.2	188.1	509.9	0.32	0.355
Ni_3V									
	0	288.7	171.2	92.3	210.3	77.0	205.9	0.37	0.337
	20	378.5	248.4	121.9	291.8	94.7	256.4	0.32	0.354
	40	489.1	327.5	153.1	381.4	118.5	322.1	0.31	0.359
	60	589.4	401.4	181.8	464.1	139.5	380.4	0.30	0.363
	80	658.2	447.7	208.7	517.9	158.6	431.7	0.31	0.361
	100	770.9	538.4	234.4	615.9	176.9	484.3	0.29	0.369

Ni_3Nb									
	0	250.3	166.6	10.6	194.5	19.1	55.5	0.1	0.452
	20	375.4	256.1	29.4	295.8	39.2	112.6	0.13	0.437
	40	470.5	321.7	45.8	371.3	55.6	158.9	0.15	0.429
	60	548.2	385.0	62.2	439.4	69.3	197.5	0.16	0.425
	80	646.0	455.4	88.6	519.0	91.2	258.5	0.18	0.417
	100	723.5	509.0	114.7	580.5	111.6	314.6	0.19	0.410

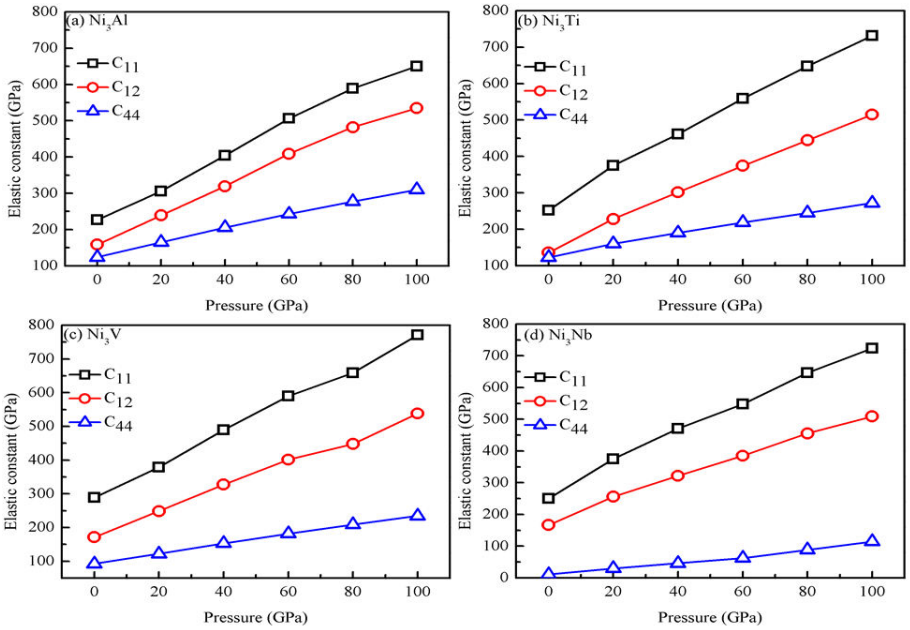

Fig.2 The elastic constants (C_{ij}) of Ni_3X (X=Al, Ti, V, Nb) at 0 to 100GPa.

The bulk modulus (B), shear modulus (G), Yong's modulus (E) and Poisson's ratio (v) of Ni_3X (X=Al, Ti, V, Nb) at 0 to 100GPa can be calculated straightforwardly by the Voigte-Reusse-Hill method[35-37], using these elastic constants from Fig.2. The calculation equations are as follows.

$$B = \frac{1}{3}(C_{11} + 2C_{12}) \tag{4}$$

$$G_V = \frac{1}{5}(C_{11} - C_{12} + 3C_{44}) \tag{5}$$

$$G_R = \frac{5(C_{11} - C_{12})C_{44}}{3(C_{11} - C_{12}) + 4C_{44}} \tag{6}$$

$$G = \frac{1}{2}(G_V + G_R) \tag{7}$$

$$E = \frac{9GB}{3B+G} \tag{8}$$

$$\nu = \frac{3B-E}{6B} \tag{9}$$

According to the methods above, the B, G, E and ν of Ni_3X (X=Al, Ti, V, Nb) at 0 to 100GPa can be obtained, as shown in Table 2 and Fig 3. It is generally accepted that *G* is usually used to measure the resistance of a metallic material to its own deformation, while *B* is used to characterize the resistance of the material to volume change.The figure clearly shows that the values of bulk modulus for different intermetallic compounds at the same pressure are much larger than the shear modulus, implying that Ni_3X tends to resist volume change more than shape change under high pressure. E is a physical quantity that describes the resistance of a solid material to deformation. It is used as a measure of the stiffness of an isotropic elastomer, the larger the E, the less deformable and more rigid the material. Thus, Ni_3Al, Ni_3Ti and Ni_3V are much stiffer than Ni_3Nb. The hardness decreases in the following order: Ni_3Ti>Ni_3V>Ni_3Al>Ni_3Nb. It is clear that the values of B, G and E in Fig.3(a), (c) show an increasing trend with increasing pressure, which indicates that pressure can increase the elastic modulus of the material and thus improve the hardness of the metal material itself. Fig. 3(b), (c), (d) show G/B, v, and A^U. Pugh [38,39] proposed a rough method for judging the toughness and tough-brittle transition behavior of materials using the ratio of G/B after an in-depth study. The brittleness of a material is associated with high G/B values, while low G/B values lead to ductility of the material [38]. The critical value of G/B to distinguish between ductility and brittleness of a material is about 0.57 [39]. Figure 3(c) shows that the calculated G/B values for different pressures are below 0.57, indicating that Ni_3Ti, Ni_3V, Ni_3Al and Ni_3Nb all show ductility. Meanwhile, the increase in pressure leads to smaller G/B values for Ni_3Al, Ni_3Ti and Ni_3V, indicating that the ductility of Ni_3X is improved at high pressure. Conversely, higher pressures resulted in worse ductility of Ni_3Nb. Poisson's ratio furnishes pertinent information on bonding capabilities [40], and for metallic materials, ν is usually between 0.25 and 0.5. the calculated values of Ni_3Al, Ni_3Ti,

Ni_3V and Ni_3Nb at different pressures are between 0.25 and 0.5, and, the Poisson's ratio values of Ni_3Al, Ni_3Ti and Ni_3V increase correspondingly with increasing pressure, which translates into better ductility of the material. On the contrary, Ni_3Nb has poor ductility.

Elastic anisotropy is an important property of materials, which reveals the difference in mechanical properties in different directions. The anisotropy of the crystal can be characterized by the universal anisotropy index. It is defined as [41,42]:

$$A^U = 5\frac{G_V}{G_R} + \frac{B_V}{B_R} - 6 \tag{10}$$

When the value of universal anisotropy index is not equal to 1, it indicates that the material is anisotropic, otherwise the crystal is isotropic. Fig.3(d) shows that the value of A^U is not equal to 1, it is obvious that Ni_3X phases are anisotropic materials. For the Ni_3X (X = Al, Ti, V) phase, the value of A^U increases with increasing external pressure, which indicates that anisotropy can be enhanced. On the contrary, the anisotropy of Ni3Nb decreases. Moreover, the anisotropy decreases in the following order at 0 GPa. Ni_3Nb>Ni_3Al>Ni_3Ti>Ni_3V. In other words, Ni_3Nb exhibits stronger anisotropy at 0 GPa than the other phases. This is closely related to its smallness C_{44} at zero pressure.

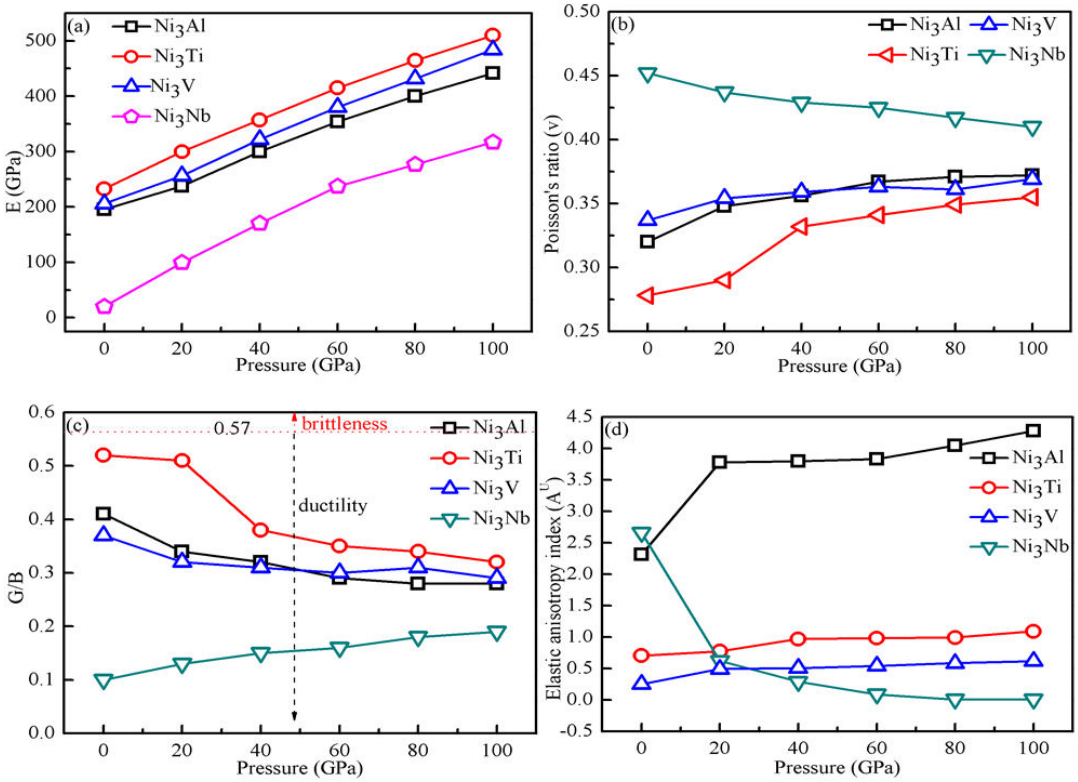

Fig.3 The function curve of pressure and Poisson's ratio, Young's modulus, bulk modulus, shear modulus and anisotropy index.

3.3 Anisotropy of acoustic velocities and Debye temperature

3.3.1 Anisotropy of acoustic velocities

The propagation of sound velocity is anisotropic in solid, which is contingent on the symmetry of the crystal structure and the direction of dissemination. The relationship is shown by the following formula [43].

$$\left|C_{ijkl}\, n_i\, n_l - \rho\upsilon^2\delta_{ik}\right| = 0 \tag{11}$$

$$\upsilon(k) = \frac{dw}{dk} \tag{12}$$

In this work, only the pure propagation modes of the cubic structure crystal Ni_3X in [100], [110], and [111] directions are considered; the sound velocities in equations (11) and (12) can be solved by the elastic constants and phonon frequencies. (13)-(16) denote the sound velocities of crystals in different crystal directions, respectively.

Cubic crystal [44,45]:

For [100] direction:

[illegible] (polarization) (13)

$$[100]\upsilon_t = \sqrt{C_{11}/\rho};[010]\upsilon_{t1} = [001]\upsilon_{t2} = \sqrt{C_{44}/\rho}; \tag{14}$$

For [110] direction:

$$\begin{aligned}&[110]\upsilon_t = \sqrt{(C_{11}+C_{12}+2C_{44})/\rho};\left[1\,\bar{1}0\right]\upsilon_{t1} = \sqrt{(C_{11}-C_{12})/\rho};\\&[001]\upsilon_{t2} = \sqrt{C_{44}/\rho}\end{aligned} \tag{15}$$

For [111] direction:

$$\begin{aligned}&[111]\upsilon_l = \sqrt{(C_{11}+2C_{12}+4C_{44})/3\rho};\\&\left[11\bar{2}\right]\upsilon_{t1} = \upsilon_{t2} = \sqrt{(C_{11}-C_{12}+C_{44})/3\rho}\end{aligned} \tag{16}$$

Where, C_{ijkl} represents the elastic constant of Ni_3X under the assumed pressure; n_i and n_l denote the polarization direction and the propagation direction of sound velocity, respectively; w is the vibration frequency of the sound wave per unit period, ν is the propagation velocity of sound (v_l: the propagation velocity of sound in the longitudinal direction, v_{tl}: is the sound velocity of the first transverse wave, and v_{t2}: the sound velocity of the second transverse wave). the calculated results of the sound velocity of Ni_3X along each direction and at varying pressures is illustrated in Fig. 4. The elastic anisotropy of the crystal can be reflected by the propagation rate of the sound velocity in different directions within the crystal. For example, C_{11} determines the longitudinal sound velocity along the [100] direction, C_{22} determines the longitudinal sound velocity along the [010] direction, C_{33} determines the longitudinal sound velocity along the [001] direction, while C_{44}, C_{55} and C_{66} determine the transverse sound velocity of Ni_3X along the [100], [010] and [001] directions, respectively.

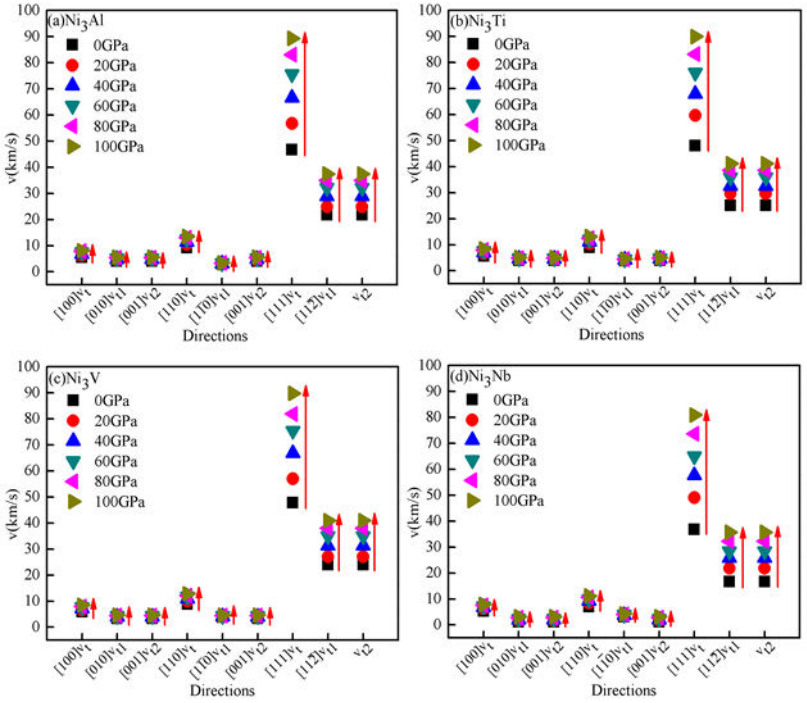

Fig.4 The sound velocity in different directions increases of the L12-type γ′-Ni3X (X=Ti, V, Nb) phase with different of pressure

In Fig.4, the outcome shows that the sound velocity in different directions increases of the $L1_2$-type γ′-Ni_3X (X=Ti, V, Nb) phase with the increase of pressure. Moreover, the speed increase rates in the [001], [110] and [111] directions are different, which indicates the existence of anisotropy of sound velocity. Among the three longitudinally propagating sound velocities in Fig.4, the longitudinal wave velocity along the [111] direction ([111] $_{Vt}$) is the fastest, which may be due to the difference of C_{11} and $_{C12}$, resulting in the difference in sound velocity propagation. This also explains the anisotropic variation of the Ni_3X phase.

3.3.2 Debye temperature

The Debye temperature (Θ_D) is an important physical parameter that reflects the degree of dynamic distortion of the solid lattice and the strength of the interatomic bond. Many physical quantities of matter are connected with it, as elasticity, hardness, specific heat and melting point, so it is essential to study the Debye temperature. Θ_D can be calculated from the data of elastic constants in Table 2 according to the following equation [46-48]:

$$\Theta_D = \frac{h}{k_B}\left[\frac{3n}{4\pi}\left(\frac{N_A\rho}{M}\right)\right]^{(1/3)}\upsilon_m \qquad (16)$$

$$\upsilon_{\mathrm{m}} = \left[\frac{1}{3} \left(\frac{2}{\upsilon_l^3} + \frac{1}{\upsilon_s^3} \right) \right]^{(-1/3)} \tag{17}$$

$$\upsilon_l = \sqrt{\frac{3B + 4G}{3\rho}} \tag{18}$$

$$\upsilon_s = \sqrt{\frac{G}{\rho}} \tag{19}$$

The h in equation (16) represents Planck's constant, K_B stands for the Boltzmann's constant, n i is the number of atoms in a single Ni_3X cell, N_A is Avogadro's number, ρ is the density of a single Ni_3X cell, M is the molecular weight of Ni_3X, respectively. υ_{m} υ_l and υ_s stand for the average, longitudinal and shear sound velocities, respectively. Table.3 displays the dependence of υ_{m}, υ_l and υ_s with pressure interval from 0 to 100GPa. The computed values of Debye temperature (Θ_D) of Ni_3X at variable pressures are demonstrated in Fig. 5. The Debye temperature of Ni_3Al and Ni_3V at 0 GPa are 461.45 K, 448.83K respectively, which is close to the existing experimental values derived from the measurement of elastic constants at chamber temperature [21]. Which are in line with the findings of this paper. It can be found that Ni_3Ti has the highest Θ_D among the five phases. Debye temperature rises with incremental pressure for Ni_3X phases, and the growth rate gradually decreases.

In addition, as mentioned above, the Debye temperature (Θ_D) can be utilized to depict the intensity of covalent bonds in solids. the larger the value of Θ_D, the stronger the covalent bonds. Therefore, the covalent bonds in Ni_3X become stronger as the pressure increases.

Table 3 Sound velocity, Debye temperature (Θ_D) of Ni_3X (X=Al, Ti, V, Nb) phases

Phase	**Pressure**	$v_m(m/s)$	$v_l(m/s)$	$v_s(m/s)$	$\Theta_D(k)$
Ni3Al	0	4207.93	6152.01	3162.58	461.45
	20	4470.68	6880.14	3317.77	490.27
	40	4849.46	7584.10	3586.32	531.81

	60	5129.87	8220.99	3775.00	562.56
	80	5340.12	8661.35	3920.81	585.61
	100	5504.08	8937.02	4040.39	603.59
Ni3Ti	0	4446.32	6132.45	3401.70	487.60
	20	4900.93	7102.18	3692.49	537.45
	40	5135.15	7660.46	3839.26	563.13
	60	5393.67	8182.37	4016.07	591.48
	80	5587.69	8605.96	4046.10	612.76
	100	5749.31	8977.2	4253.29	630.48
Ni3V	0	4092.86	3053.58	6156.80	448.83
	Other calculation [21]	3835.20	3432.78	6442.70	507.12
	20	4442.07	3288.78	6909.67	487.13
	Other calculation [21]	4196.65	3648.77	7248.24	570.23
	40	4809.94	3551.61	7578.06	527.47
	60	5088.3	3749.84	8094.33	558.00
	80	5300.28	3910.35	8385.85	581.24
	100	5516.44	4054.6	8896.58	604.95
Ni3Nb	0	2079.96	1466.94	4981.47	228.09
	20	2835.67	2015.41	6005.79	310.97
	40	3263.52	2328.63	6588.92	357.89
	60	3557.53	2542.98	7043.09	390.13
	80	3976.12	2853.68	7563.29	436.03
	100	4302.19	3099.52	7922.38	471.85

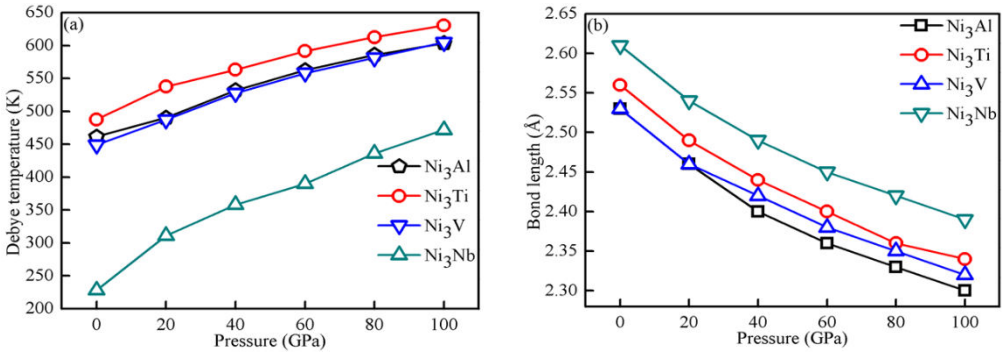

Fig.5 Sound velocity, Debye temperature (Θ_D) of Ni_3X (X=Al, Ti, V, Nb) phases

3.4 Electronic structure

To in addition recognize the bonding traits and to look into the impact of stress on the digital structure, the whole density of states and partial density of states of Ni_3X are calculated in this paper, as proven in Fig. 6. Here it is solely the TDOS of Ni_3X at 0, 40 and 80 GPa that it has plotted to describe the hassle extra clearly.

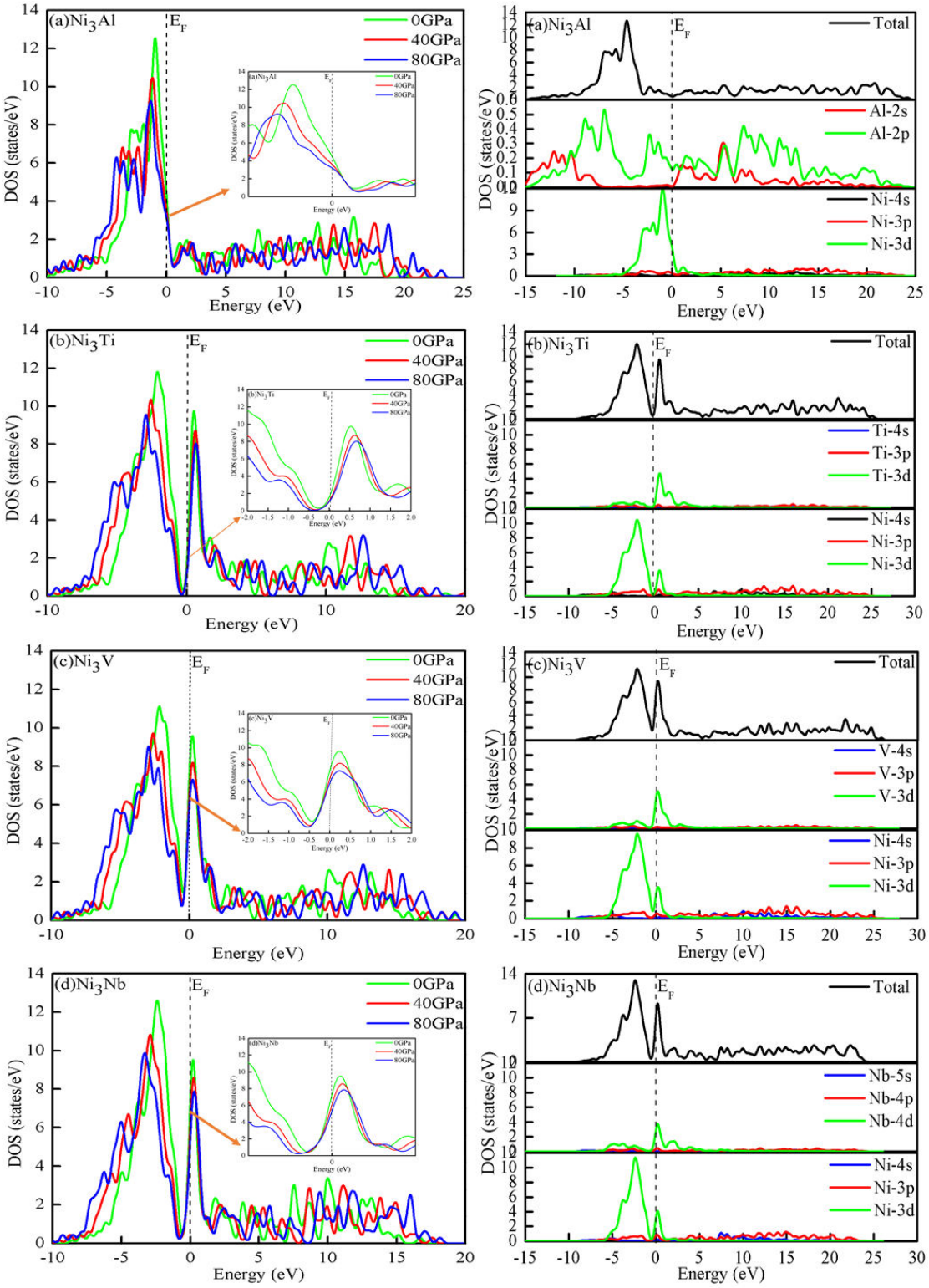

Fig.6 Density of states of Ni_3X (X=Al, Ti, V, Nb) at 0,40,80GPa.

As seen in Fig. 6, many energy states occupy the Fermi level, which means that the Ni_3X phase demonstrates metallic properties. In addition, the peak height of TDOS can be significantly reduced by increasing the pressure, and the distribution range of TDOS can be expanded. For Ni_3Al, Ni_3Ti, Ni_3V and Ni_3Nb, the dominant

bond-forming peaks in the vicinity of the Fermi level are dominated by the Ni-3d and Al-3p states, the Ni-3d and Ti-3d states, and the Ni-3d and V-3d states. In particular, the hybridization between Ni and X atoms is apparent, which forms a covalent bonding feature.

To reap perception into the chemical bonding homes of Ni_3X beneath pressure, Mulliken charges [49] as properly as bond lengths have been analyzed to quantitatively examine the impact of stress on structural, elastic, thermodynamic, and digital properties. The ionic configurations are listed in Table 4. At 0 GPa, the charges transferred from X to Ni atoms for Ni_3Al, Ni_3Ti, Ni_3V, and Ni_3Nb are 0.25, 0.40, 0.30, and 0.28 e, respectively. In addition, the charges transferred from X to Ni atoms expand with growing pressure. But the bond length size decreases with the ascend of pressure. This is the physical root of the impact of pressure on the structure, elastic constants and Debye temperature, etc. This offers an appropriate rationalization for the variant of lattice constant and volume with pressure.

Table 4 Mulliken Charge, Bond length of Ni_3X (X=Al, Ti, V, Nb) phases at 0 to 100GPa

Pressure	Ni_3Al		Ni_3Ti		Ni_3V		Ni_3Nb	
(GPa)	Bond length (Å)	Mulliken Charge(e)	Bond length (Å)	Mulliken Charge(e)	Bond length (Å)	Mulliken Charge(e)	Bond length (Å)	Mulliken Charge(e)
0	2.53	$Ni^{-0.08}Al^{+0.25}$	2.56	$Ni^{-0.13}Ti^{+0.4}$	2.53	$Ni^{-0.1}V^{+0.3}$	2.61	$Ni^{-0.09}Nb^{+0.28}$
20	2.46	$Ni^{-0.07}Al^{+0.22}$	2.49	$Ni^{-0.2}Ti^{+0.59}$	2.46	$Ni^{-0.15}V^{+0.44}$	2.54	$Ni^{-0.19}Nb^{+0.58}$
40	2.4	$Ni^{-0.06}Al^{+0.19}$	2.44	$Ni^{-0.26}Ti^{+0.78}$	2.42	$Ni^{-0.19}V^{+0.58}$	2.49	$Ni^{-0.29}Nb^{+0.86}$
60	2.36	$Ni^{-0.05}Al^{+0.16}$	2.4	$Ni^{-0.32}Ti^{+0.96}$	2.38	$Ni^{-0.24}V^{+0.72}$	2.45	$Ni^{-0.37}Nb^{+1.11}$
80	2.33	$Ni^{-0.04}Al^{+0.13}$	2.36	$Ni^{-0.38}Ti^{+1.14}$	2.35	$Ni^{-0.29}V^{+0.86}$	2.42	$Ni^{-0.45}Nb^{+1.35}$
100	2.3	$Ni^{-0.03}Al^{+0.10}$	2.34	$Ni^{-0.44}Ti^{+1.31}$	2.32	$Ni^{-0.33}V^{+0.99}$	2.39	$Ni^{-0.53}Nb^{+1.58}$

To further analyze the difference interaction between Al, Ti, V, Nb atoms and Ni atoms, this article studies the charge density (Fig 7 is the charge density diagram of Ni_3X phases.) distribution of Ni_3X on the [010] crystal plane. From the point of view of electron transfer between atoms, Ni atoms lose more electrons in Ni_3X (X=Ti, V, Nb), and the lost electrons are transferred to the space between Ni atoms and Ti, V, and Nb (the red part in Fig 7). With the pressure increases, the electron transfer tendency increases. The order of electron aggregation strength between doping atoms is Ti>Nb>V>Al, therefore, the interaction between Ti atoms and Ni atoms is the

strongest, and the interaction between Ta atoms and Ni atoms is the weakest. This is consistent with the analysis results of the enthalpy of formation, the Debye temperature and the density of states.

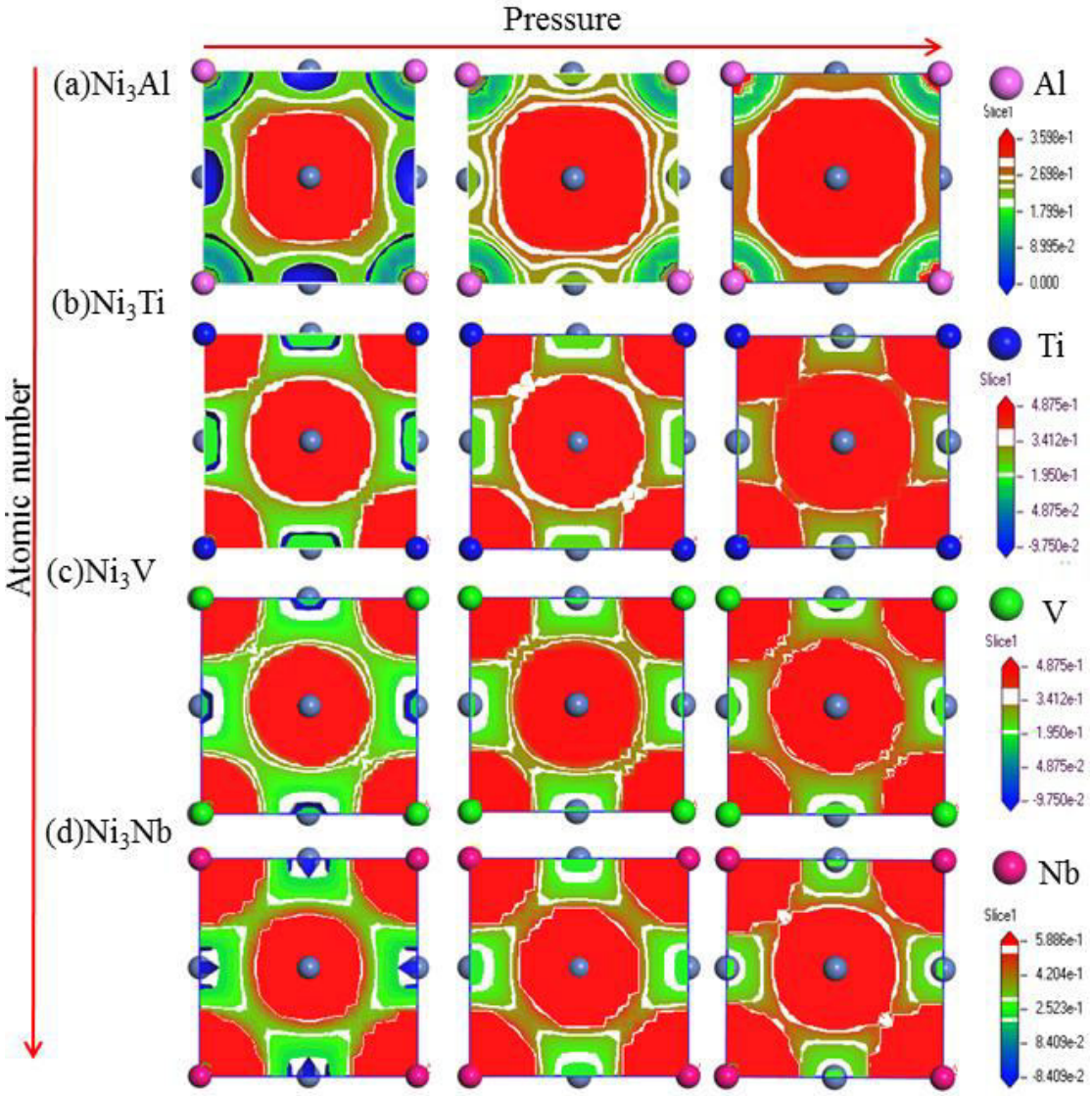

Fig.7 The charge density of Ni_3X (X=Al, Ti, V, Nb) at 0,40,80GPa.

4 Conclusion

In this paper, the structural stability(ΔH), elastic constants(C_{ij}), bulk modulus (B), Yong's modulus (E), shear modulus (G), Debye temperature (Θ_D), and electronic structures of L12-type Ni3X (X=Al, Ti, V, Nb) phases under external pressure condition were systematically studied by first principles calculations. The conclusion is as follows:

(1) The relationship between elastic constant, elastic modulus, G/B value and

Poisson's ratio under pressure shows that Ni_3X has good shear stability and ductility. And the C_{ij}, *B, G, E* values increase with the increase of pressure.

(2) All Ni_3X phases have the sound velocity anisotropy, and the increase of external pressure leads to the enhancement of anisotropy. The [111] direction has strong longitudinal anisotropy, which is closely related to the large C_{ij} of Ni_3X phases.

(3) The sound velocity and Debye temperature increase of the Ni_3X phases with the increase of the applied pressure. The magnitude of the Debye temperature under the applied pressure is: Ni_3Ti> Ni_3Al >Ni_3V> Ni_3Nb.

(4) Electronic analysis shows that increase pressure results in improving the bond strength and crystal stability of Ni_3X phases. The degree of charge hybridization and Ni-X bond strength increases with increasing pressure. In those phases, the charge accumulation of Ni_3Ti is the largest and the crystal structure is the most stable.

Acknowledgement

This project is supported by National Natural Science Foundation of China (Grant No. 51805316), China postdoctoral Science Foundation (No.2019M651491), State Key Laboratory of Advanced Welding and Joining (No. AWJ-20-M12), Shanghai Local Universities Capacity Building Project of Science and Technology Innovation Action Program (20030500900) and Shanghai sailing program (No. 21YF1432300). The computations were done on the high performance computers of the Advanced Computing Center of Yunnan University.

Declarations

Conflicts of interest： The authors declare that they have no conflict of interest.

Availability of data and material

The raw/processed data required to reproduce these findings can be shared upon request.

Code availability

The code for the simulations can be provided upon request.

Authors' contribution： **Y H Wu**: Investigation, Methodology, Formal analysis, Validation, Writing - original draft, Writing - review & editing. **J S Chen:** Writing - review & editing, Validation. **J Y Ji**: Formal analysis, Methodology, Validation. **Y Z Zhang**: Conceptualization, Methodology. **Q Z Wang**: Writing - review & editing. **K Xiong**: Conceptualization, Methodology.

References

[1] Reed R C, Tao T, Warnken N. Alloys-by-design: application to nickel-based single crystal superalloys[J]. Acta Materialia, 2009, 57(19): 5898-5913.

[2] Shiyu Ma. Study on Microscopy and Simulation Calculation of TCP Phase and Dislocations in Nickel-Based Single Crystal Superalloys[D].2018.

[3] Tan Z H, Wang X G, Song W, et al. Oxidation behavior of a novel Nickel-based single crystal superalloy at elevated temperature[J]. Vacuum, 2020, 175:109284.

[4] Wang Z, Wu W, Liang J, et al. Creep–fatigue interaction behavior of nickel-based single crystal superalloy at high temperature by in-situ SEM observation[J]. International Journal of Fatigue, 2020:105879.

[5] P Li. Electron Microscopy Analysis and First-Principles Study of Precipitated Phases in Nickel-based Single Crystal Superalloys[J].2020.

[6] Dong C, Yu J, Xu L, et al. Tension–compression asymmetry of bilayer Ni/Ni3Al affected by dislocation formation–decomposition and twinning size[J]. Materials Express, 2020.

[7] C G Liu, Y S Zhao, Jian Zhang, et al. The effect of stress aging on the precipitation behavior of TCP phase in DD11 single crystal superalloy[J]. Materials for Mechanical Engineering, 2018, 42(6).

[8] Yang Z W, Lian J, Cai X Q, et al. Microstructure and mechanical properties of Ni_3Al-based alloy joint transient liquid phase bonded using Ni/Ti interlayer[J]. Intermetallic, 2019, 109:179-188.

[9] JS A, HX C, L BW, et al. Microstructure and oxidation behaviour of Pt modified NiCrAlYSi coating on a Ni-based single crystal superalloy - ScienceDirect[J]. Surface and Coatings Technology, 2020, 399.

[10] Yang F M, Lian L X, Liu Y, et al. Mechanism of adding rhenium to improve hot corrosion resistance of nickel-based single-crystal superalloys[J]. Rare Metals, 2020:1-7.

[11] YY Huang. Study on the influence of refractory metal elements on the precipitation behavior of model Ni-Al-Cr-based superalloys[D]. 2016.

[12] Yi Chen. Correlation of Re-W alloying in nickel-based single crystal superalloys and analysis of its synergistic strengthening and toughening effect on γ′-Ni_3Al phase[D].

[13] CY Yao, Z Chen, Jing Zhang, et al. The effect of Ta alloying on the elastic properties and electronic structure of γ-Ni_3Al phase[J]. Rare Metal Materials and Engineering, 2013, 42(9):1893-1896.

[14] Li P, Zhang J, Zhang Y, et al. Density functional theory calculations of the double gamma prime Ni_3Ta phase under pressure: Structural, mechanical, and electronic properties[J]. Journal of Physics and Chemistry of Solids, 2019, 138:109248.

[15] K Santhy, Vamsi K V, Karthikeyan S. Modelling of Ni_3(Ti，V) system through first-principles calculations[J]. Materials Today: Proceedings, 2019, 26.

[16] Czeppe, T., Wierzbicka-Miernik, A., Sypien, A. et al. Effects of Ti and High Cooling Rate on the Phase Equilibria and Properties of Ni_3(Al,V) Alloys. J. of Materi Eng and Perform 29, 1502–1508 (2020). https://doi.org/10.1007/s11665-019-04527-9

[17] X Gong, WW Xu, C Cui, et al. Exploring alloying effect on phase stability and mechanical properties of γ″-Ni_3Nb precipitates with first-principles calculations - ScienceDirect[J]. Materials & Design, 2020, 196. [18] Hou H, Wen Z, Zhao Y, et al. First-principles investigations on structural, elastic, thermodynamic and electronic properties of Ni_3X (X = Al, Ga and Ge) under pressure[J]. Intermetallics, 2014, 44(1):110-115.

[19] Mao P, Yu B, Liu Z, et al. First-principles investigation on mechanical, electronic, and thermodynamic properties of Mg2Sr under high pressure[J]. Journal of Applied Physics, 2015, 117(11):115903.

[20] Liu Y, Hu W C, Li D J, et al. First-principles investigation of structural and electronic properties of $MgCu_2$ Laves phase under pressure[J]. Intermetallics, 2012, 31(none):257-263.

[21] Zhao, Yuhong. The structural, elastic, electronic properties and Debye temperature of $D0_{22}$-Ni_3V under pressure from first-principles. [J]. Journal of Alloys & Compounds, 2015.

[22] Chen Z, Zhang P, Chen D, et al. First-principles investigation of thermodynamic, elastic and

electronic properties of Al_3V and Al_3Nb intermetallics under pressures[J]. Journal of Applied Physics, 2015, 117(8):085904.

[23] Wu Q, Li S. Alloying element additions to Ni3Al: Site preferences and effects on elastic properties from first-principles calculations[J]. Computational Materials Science, 2012, 53(1):436-443.

[24] P. Hohenberg, W. Kohn, Physical Review 136 (1964) B864.

[25] J.P. Perdew, K. Burke, M. Ernzerhof, Physical Review Letters 77 (1996) 3865.

[26] Head J D, Zerner M C. A Broyden—Fletcher—Goldfarb—Shanno optimization procedure for molecular geometries[J]. Chemical Physics Letters, 1985, 122(3):264-270.

[27] Rao PM, Suryanarayana S, Murthy KS, Naidu SN. J Phys Condens Matter 1989; 1:5357.

[28] Guo G, Wang Y, Hsu LS. J Magn Magn Mater 2002; 239:91

[29] R. Boulechfar, H. Meradji, Z. Chouahda, S. Ghemid, S. Drablia, R. Khenata, FP- LAPW investigation of the structural, electronic and thermodynamic properties of Al3Ta compound, Int. J. Mod. Phys. B 29 (2015).

[30] R. E. Watson and M. Weinert, Phys. Rev. B 58, 5981–5988 (1998).

[31] H. Hu, X.Z. Wu, R. Wang, Z.H. Jia, W.G. Li, Q. Liu, Structural stability, mechanical properties and stacking fault energies of TiAl3 alloyed with Zn, Cu, Ag: first- principles study, J. Alloys Compd. 666 (2016) 185–196.

[32] Ravindran P, Fast L, Korzhavyi P A, et al. Density functional theory for calculation of elastic properties of orthorhombic crystals: Application to $TiSi_2$[J]. Journal of Applied Physics, 1998, 84(9):4891-4904.

[33] Fecht H J, Wunderlich, Battezzati, et al. Thermophysical properties of materials[J]. Europhysics news, 2008, 39(5):19-21.

[34] ZB Li, X K, Jin C C, et al. Structural, mechanical, thermodynamic and electronic properties of Pt_3M (M = Al, Co, Hf, Sc, Y, Zr) compounds under high pressure[J]. Rare Metals, 2021(3).

[35] R. Hill, The elastic behaviour of a crystalline aggregate, Proc. Phys. Soc. 65 (1952) 349–354.

[36] W. Voigt, Lehrbuch Der Kristallphysik, Taubner, Leipzig, 1928.

[37] A. Reuss, Z. Angew, Calculation of the flow limits of mixed crystals on the basis of the plasticity of monocrystals, Math. Mech. 9 (1929) 49.

[38] S.F. Pugh, XCII. Relations between the elastic moduli and the plastic properties of

polycrystalline pure metals, Philos. Mag. 45 (2009) 823–843

[39] Pugh S. Phil Mag Ser 1954; 45:823

[40] Nye JF. Physical properties of crystals: their representation by tensors andmatrices. NewYork: Oxford University Press; 1985.

[41] S.I. Ranganathan, M.J.P.R.L. Ostoja-Starzewski, Universal Elastic Anisotropy Index, vol. 101, 2008, 055504

[42] Cao Y, Zhang C, Zhou S, et al. First-principles study of stability, electronic properties and anisotropic elasticity of Al3M (M=Ti, Ta, V, Nb, Hf) intermetallic compounds[J]. Physica B Condensed Matter, 2020, 594:412294.

[43] Grimvall G. Thermophysical properties of materials, North Holland. Amsterdam: Elsevier B. V; 1999.

[44] Feng J, Xiao B, Chen J, et al. Stability, thermal and mechanical properties of Pt_xAl_y compounds[J]. Materials & Design, 2011, 32(6):3231-3239.

[45] Hearmon R F S, Maradudin A A. An Introduction to Applied Anisotropic Elasticity[J]. Physics Today, 1961, 14(10):48-48.

[46] Anderson OL. J Phys Chem Solids 1963; 24:909.

[47] Huang ZW, Zhao YH, Hou H, Han PD. Phys B Condens Matter 2012;407:1075.

[48] Shang S L, Wang Y, Kim D E, et al. First-principles thermodynamics from phonon and Debye model: Application to Ni and Ni_3Al[J]. Computational Materials Science, 2010, 47(4):1040-1048.

[49] Larin A. Approximations of the Mulliken charges for the oxygen and silicon atoms of zeolite frameworks calculated with a periodic Hartree–Fock scheme[J]. International Journal of Quantum Chemistry, 2010, 70(4-5):993-1001.